designs

MDPI

Article

Suitability of Electrical Coupling in Solar Cell Thermoelectric Hybridization

Bruno Lorenzi [1,2,*], Maurizio Acciarri [1] and Dario Narducci [1]

[1] Department of Materials Science, University of Milano Bicocca, via R. Cozzi 55, 20125 Milano, Italy; maurizio.acciarri@unimib.it (M.A.); dario.narducci@unimib.it (D.N.)
[2] Department of Mechanical Engineering, Massachusetts Institute of Technology, Cambridge, MA 02139, USA
* Correspondence: bruno.lorenzi@unimib.it; Tel.: +39-02-6448-5168

Received: 8 August 2018; Accepted: 6 September 2018; Published: 8 September 2018

Abstract: It is well known that the major constraints to the efficiency of photovoltaic devices come from the generation of heat. In this context, thermoelectric generators have been proposed as a viable heat recovery solution, leading to an increase of the overall efficiency. Within this kind of hybrid solution, the photovoltaic and thermoelectric parts can be either electrically separated or connected in the same circuit. In the latter case, the presence of the thermoelectric generator in series to the solar cell may lead to electrical losses. In this work, we analyze the effect of several parameters on the output power of electrically hybridized thermoelectric-photovoltaic systems. Both electrical measurements and simulations are used. The results show that while an electrical lossless condition exists (as also reported in previous works), it does not necessarily lead to significant power gains compared to the sole photovoltaic case. In addition, the strong temperature sensitivity of the lossless condition makes electrical hybridization difficult to implement. Since solar irradiation varies over time, such sensitivity would make the system work mostly in a suboptimal regime. Therefore, this study provides clues on the actual applicability of electrically hybridized devices.

Keywords: photovoltaics; thermoelectrics; electrical hybridization

1. Introduction

It is well known that the major constraints to photovoltaic (PV) efficiency, especially in single-junction solar cells, come from the spontaneous generation of a considerable amount of heat within the device. Therefore, thermal recovery strategies could be used to increase the overall solar harvesting efficiency. In some cases, heat is recovered as such, through the co-generation of warm water [1–3]. Other approaches focus instead on the conversion of heat into electricity with the implementation of thermoelectric generators (TEGs) [4–7] through hybrid thermoelectric-photovoltaic systems (HTEPV).

The latter solution has attracted much interest in the solar harvesting community, leading to the publication of an increasing number of theoretical [8–12] and experimental works [13–16], and of a book as well [17]. In general, HTEPV systems can be either optically or thermally coupled. In the case of optically coupled devices (OC), a beam splitter is used to separate the light absorbed by the PV (the ultra-violet and visible part of the spectrum) from that absorbed by the TEG (the infra-red portion). In this case, the PV cell temperature is independent of that of the TEG. In thermally coupled (TC) systems, instead, the PV and TEG parts are in thermal contact, and the PV cell temperature is normally considered to be equal to that of the TEG hot side. At first glance, OC systems may be expected to have higher efficiencies compared to TC ones, because the TEG temperature may be increased without affecting the PV efficiency. However, we showed elsewhere [18,19] that OC systems are actually less efficient in converting solar power into heat flowing through the TEG.

Furthermore, irrespective of the thermal pairing strategy, the PV and TEG parts can be either electrically separated or connected to the same output circuit. In the former case, the two stages feed separate electric loads, so that the HTEPV output power is simply the sum of the PV and TEG contributions. In the latter case, instead, since the PV and TEG parts are electrically connected to the same circuit, the overall efficiency is not simply the sum of the two contributions since the series resistance of the TEG is detrimental to the PV efficiency, leading to electrical losses.

In this view, non-electrically hybridized devices could be seen as preferable. However, since the TEG efficiency is small, it is arguable whether a small thermoelectric power output may be of any practical use when not connected to a larger PV output, forcing researchers to reconsider electric hybridization.

In the literature, several works have focused on the electrical hybridization of HTEPV devices. Specifically, Fisac et al. [20] and Park et al. [21] analyzed silicon solar cells. Fisac et al. reported experimental and theoretical results of the hybridization of a silicon panel, showing a small increase of the overall efficiency when operating at 55 °C. Unfortunately, the lack of details on the experimental procedure and on the thermoelectric generators used in their work makes it difficult to generalize their results. Park et al. considered instead a silicon solar cell hybridized with three different TEGs having different internal resistances, contributing to an advancement of the understanding of the role of electrical losses in HTEPV devices. However, in this case their conclusions cannot be extended beyond the case of silicon PVs and to a specific set of TEGs. Similar remarks also apply to the interesting papers by Li et al. [22] and by Verma et al. [23]. The former discussed the optimal load resistance for the case of hybridized GaAs and silicon solar cells, and the latter proposed a maximum power point tracking (MPPT) system. Finally, in a very recent paper, Xu et al. [16] proposed the electrical hybridization of a perovskite solar cell using four to 10 TEGs, all connected in series to the PV stage, and they reported a strangely small electrical loss despite the large number of TEGs in connected series with the solar cell.

Overall, it seems sensible to conclude that a more comprehensive investigation of the interplay between the PV series resistance, the TEG resistance, and the optimal harvester working temperature may be needed.

In this work, we try to cover this gap by analyzing the effect of the many parameters that come into play, using both electrical measurements and simulations.

2. Materials and Methods

As already mentioned, OC and TC hybrid systems can be either electrically separated or connected in the same circuit. In the first case the two parts are connected to different electric loads, thus the HTEPV output power is simply the sum of the PV and TEG contributions:

$$P_{htepv} = P_{pv} + P_{teg} \tag{1}$$

where

$$P_{pv} = V_{pv}^{oc}\, I_{pv}^{sc}\, FF_{pv} \tag{2}$$

and

$$P_{teg} = \frac{V_{teg}^2}{4\, R_{i,teg}} \tag{3}$$

with V_{pv}^{oc}, I_{pv}^{sc}, and FF_{pv} respectively denoting the open-circuit voltage, the short-circuit current, and the filling factor of the solar cells. V_{teg} and $R_{i,teg}$ respectively represent the thermoelectric voltage and the thermoelectric generator internal resistance.

In the second case, the presence of the TEG in electric series with the PV cell may lead to electrical losses due to the increase of the PV series resistance. Thus, for the electrically hybridized HTEPV device, the power output reads:

$$P_{htepv}^{el} = P_{pv} + P_{teg} - P_{loss} \tag{4}$$

As shown by Park et al. [21], for a given $R_{i,teg}$, a V_{teg} exists (and thus a temperature difference at the TEG sides) that allows the HTEPV device to work in an electrical lossless condition (i.e., for which P_{loss} is negligible). However, it must be pointed out that either for lower or higher values of V_{teg}, this lossless condition is no longer fulfilled. In addition, it is also clear that the interplay between the PV series resistance and $R_{i,teg}$ sets the optimal V_{teg} needed, thus revealing the convenience of this approach. A systematic analysis of such an interplay is still missing, however.

To properly investigate the electrically coupled system, we analyzed the influence of the TEG addition by means of the simulator shown in Figure 1.

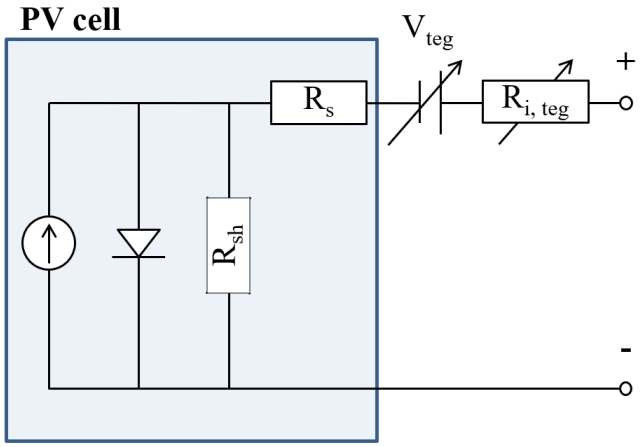

Figure 1. Scheme of the simulator used in this work. Several types of photovoltaic (PV) cells were connected in series with a voltage generator and a variable electrical resistance.

In this circuit, a real solar cell under illumination is placed in series with a voltage generator and a variable electrical resistance. Changing both the generated voltage and the electrical resistance, we recorded the variation of the solar cell current-voltage (IV) characteristics.

Using the simulator, we analyzed the electrical hybridization of four commercial silicon PV cells having different values of R_s. Setting $R_{i,teg}$ as a multiple of R_s, V_{teg} was changed until the electrical lossless condition was reached:

$$P_{loss} = 0 \tag{5}$$

or equivalently:

$$\frac{P^{el}_{htepv}}{P_{htepv}} = 1 \tag{6}$$

We will refer hereafter to the condition of Equation (6) as the electrical lossless condition. Please note that the choice of setting $R_{i,teg}$ as an integer multiple of R_s is arbitrary and was made only to easily catch the relation between the two resistances. In principle, $R_{i,teg}$ may take any value.

In addition, the IV curves were fitted using the following equation [21], which is the single diode equation for the solar cell accounting for the addition of the TEG in the same circuit:

$$I^{el}_{htepv} = I^{sc}_{pv} - I^{0}_{pv} \exp\left[\frac{V - V_{teg} + I^{el}_{htepv}(R_s + R_{i,teg})}{n\,\kappa\,T_{cell}}\right] - \frac{V - V_{teg} + I^{el}_{htepv}(R_s + R_{i,teg})}{R_{sh}} \tag{7}$$

where I^{0}_{pv}, n, κ, T_{cell} and R_{sh} respectively represent the recombination current, the solar cell ideality factor, the Boltzmann constant, the cell temperature, and the solar cell shunt resistance. In our approach, the values of R_s and R_{sh} were extrapolated with standard methods [24], leaving n and I^{0}_{pv} as the only unknown parameters to be fitted.

Interestingly enough, the simulator of Figure 1 does not consider the temperature sensitivity of the solar cell, and therefore it better models the behavior of OC systems. In fact, as mentioned,

in this case the temperature of the solar cell can be considered as independent of the TEG temperature, and therefore was set equal to room temperature. Thus, the thermoelectric hybridization is here always beneficial to the overall power output (if optical losses due to the splitting strategies are small). Instead, for TC systems this is not necessarily true. Therefore, to generalize our analysis, the solar cell temperature sensitivity was accounted for as follows.

Let us first define the thermoelectric power gain as:

$$G_p = \frac{P_{htepv}}{P^0_{pv}} \tag{8}$$

where P^0_{pv} is the sole PV output power at room temperature. Thermoelectric hybridization is convenient when G_p is larger than 1. It should be stressed that electrical lossless conditions and power gain are independent of each other. For example, for very temperature-sensitive solar cells, G_p is actually expected to be always smaller than 1. In this case, while the thermoelectric power output could be high enough to obtain the electrical lossless condition (especially for TEGs with small internal resistances), one would never obtain $G_p \geq 1$.

Based on the very good agreement between the measured IV curves and those calculated by Equation (7), we performed numerical simulations to compute G_p values in the lossless condition for the case of amorphous silicon (a-Si) and copper zinc tin sulfide (CZTS) solar cells. The reason behind the choice of these materials is reported in previous publications [18,19]. The case of crystalline and polycrystalline silicon is not examined in this work since the temperature sensitivity of silicon PV efficiency is too high to enable an efficient hybridization [25], unavoidably leading to a value of G_p smaller than 1. For a-Si and CZTS solar cells, instead, pairing with thermoelectrics has been shown to be promising because of their smaller temperature sensitivity.

Therefore, starting from state-of-the-art room temperature IV curves, and using parameters reported in the literature for these two materials [26–29], we extrapolated R_s and R_{sh} values. Then we used Equation (7) (with $V_{teg} = R_{i,teg} = 0$) to fit the IV curves to obtain I^0_{pv} and n at room temperature. The solar cell IV as a function of the temperature was finally computed by considering the temperature dependency of the recombination current [30]:

$$I^0_{pv} = B\, T^3_{cell}\, \exp\left(\frac{E_g}{\kappa\, T_{cell}}\right) \tag{9}$$

where B is a parameter independent of the temperature obtained from the I^0_{pv} at room temperature, and E_g is the material energy gap. All other parameters of Equation (7), including E_g and n, were considered independent of temperature.

To validate this procedure, we first calculated the solar cell power output as a function of temperature and then used the following equation to extrapolate the so-called efficiency temperature coefficient β^0_{pv}, to be compared with the experimental values reported in the literature [31,32] (see Table 1):

$$P_{pv}\,(T) = P^0_{pv}\left[1 + \beta^0_{pv}\,(T - T_a)\right] \tag{10}$$

with $T_a = 300$ K.

Finally, using Equation (7) (with V_{teg} and $R_{i,teg} \neq 0$), we obtained P^{el}_{htepv} as a function of $R_{i,teg}$ and V_{teg} Specifically, for any fixed $R_{i,teg}$ value we moved V_{teg} by changing the solar cell temperature between 300 and 500 K, assuming that:

$$V_{teg} = n_{leg}\, S_{teg}(T_{cell} - T_a) \tag{11}$$

where n_{leg} and S_{teg} respectively denote the number of thermoelectric couples per unit area and the Seebeck coefficient of one thermoelectric couple. In this work, we assume $n_{leg}\, S_{teg} = 0.0065\ \mathrm{V{\cdot}K^{-1}{\cdot}cm^{-2}}$, which is a typical value for commercially available TEGs. In Equation (9), we also implicitly assumed that the

TEG hot side temperature was equal to T_{cell} and that a thermal dissipation system at the TEG cold side could maintain the cold side temperature at T_a.

Table 1. Parameters for numerical simulations.

Solar Cell	P^0_{pv} (mW/cm^2)	fi^0_{pv} (%/K)	fi^0_{pv} calc. (%/K)	R_s (Ω·cm^2)
Amorphous Silicon (a-Si)	101.89 [26]	0.150 [31]	0.146	5.50
Copper Zinc Tin Sulfide (CZTS)	89.84 [27]	0.170 [32]	0.174	4.01

3. Results

In this section we report the results of the analysis described above on the electrical hybridization of silicon, a-Si, and CZTS solar cells.

In the first subsection, we describe what was obtained with silicon solar cells by means of the simulator reported in Figure 1, while the second subsection is dedicated to the simulations performed on a-Si and CZTS solar cells.

3.1. Lossless Conditions

Figure 2 summarizes the effect of $R_{i,teg}$ and V_{teg} on the IV curve of a given solar cell (black line in Figure 2), recorded with the simulator depicted in Figure 1. The plot shows that the effect of $R_{i,teg}$ is to decrease the solar cell filling factor (for moderate values of $R_{i,teg}$) or to decrease I^{sc}_{pv} (for high values of $R_{i,teg}$), consistent with what expected from the variation of the solar cell series resistance. The open-circuit voltage changes instead when a V_{teg} is applied, giving:

$$V^{oc}_{htepv} = V^{oc}_{pv} + V_{teg} \tag{12}$$

This is in line with what was reported in previous electrical hybridization studies [9,16,20–23]. The behavior shown in Figure 2 also indicates that there is a minimum V_{teg} (and therefore a minimum ΔT) capable of compensating the decrease of the PV filling factor, giving thus $G_p = 1$. At higher values of V_{teg}, the hybridization gain with respect to the sole PV case increases, and thus $G_p > 1$. However, we stress that the minimum V_{teg} to obtain $G_p = 1$ is generally different from the V_{teg} needed for lossless conditions.

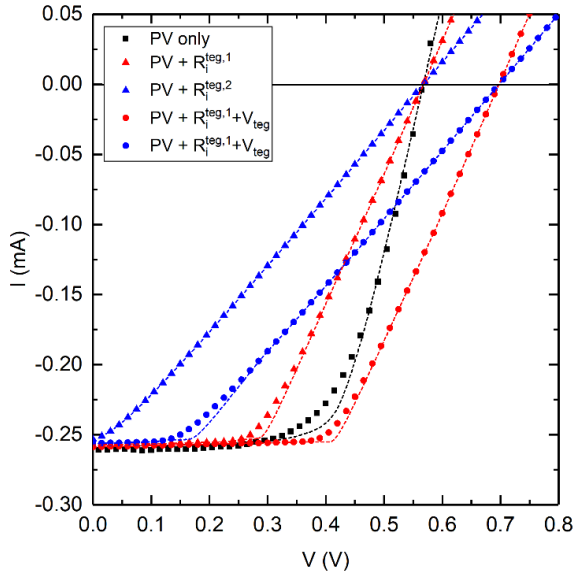

Figure 2. Example of the effect of $R_{i,teg}$ (red and blue triangles) and the combination of $R_{i,teg}$ and V_{teg} (red and blue circles) on the solar cell current-voltage (IV) curve of a solar cell (black squares). Dashed lines are fits from Equation (7). In this example, $R^1_{i,teg} < R^2_{i,teg}$.

Figure 2 also compares the experimental measurements made with the simulator of Figure 1 (blue and red circles) to the simulations calculated using Equation (7), showing that the computed IV curves fit the measurements very well. While the values for I^{el}_{htepv} and V^{oc}_{htepv} are exact up to the third significant digit, the values of the output power P^{el}_{htepv} are less precise. The reason for this is that we fit the solar cell with a simple single diode equation instead of a multiple diode equation. However, the computed P^{el}_{htepv} always differs from the actual power output by less than 5%.

Finally, Figure 3 reports the results of the measurements carried out using the simulator shown in Figure 1. On the left side we report the effect of $R_{i,teg}$ on four silicon solar cells, monitoring the variation of G_p as a function of $R_{i,teg}$. As expected, we found that increasing $R_{i,teg}$ causes G_p to decrease in all cases.

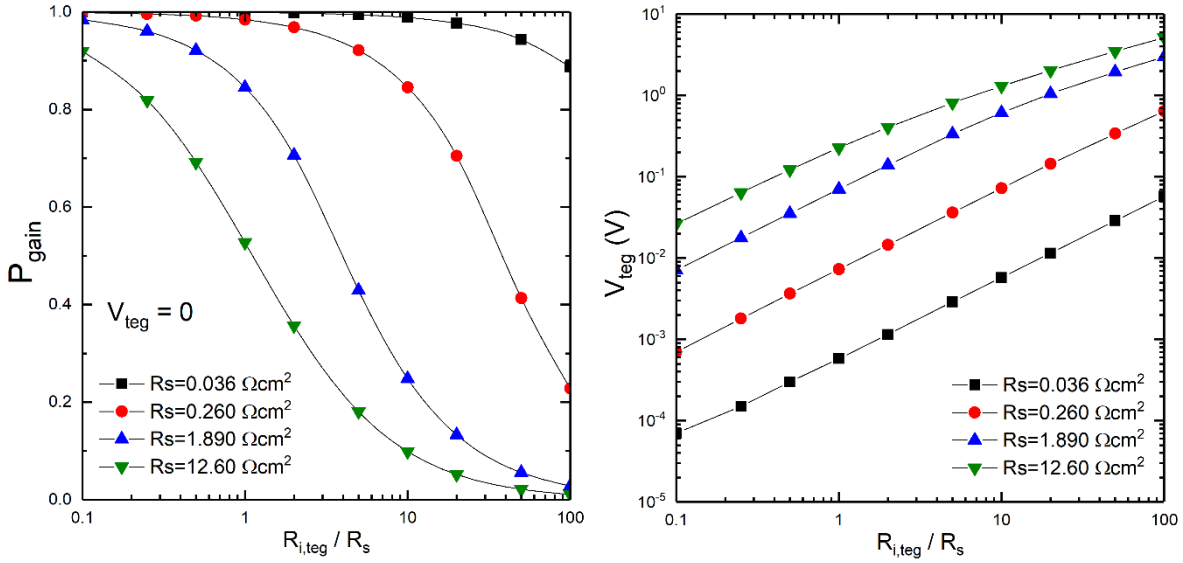

Figure 3. (**Left**) Effect of $R_{i,teg}$ on the solar cell power in the case of $V_{teg} = 0$. (**Right**) V_{teg} needed for a lossless condition.

Furthermore, we found that solar cells with a small value of R_s better withstand high $R_{i,teg}$ values. Thus, the smaller the solar cell series resistance, the smaller the V_{teg} needed to reach the electrical lossless condition (equivalent to $G_p = 1$, since in this case temperature sensitivity is not taken into account). We also found that the V_{teg} for lossless conditions increases linearly by increasing $R_{i,teg}$ with a fixed slope for small values of R_s (black and red lines in Figure 3, right), while it displays a non-linear behavior for larger R_s (blue and green lines).

3.2. G_p vs Lossless Conditions

In Table 1, we report the values of P^0_{pv} and β^0_{pv} found in the literature along with the values of β^0_{pv} calculated according to the procedure outlined in the previous section and the extrapolated solar cell series resistances. The calculated and literature values of β^0_{pv} were found to be in good agreement.

Figure 4 reports the interplay between electrical losses and G_p for the two materials considered in this work. As expected, the electrical lossless condition (meaning a value equal to one on the y axis) does not correspond to $G_p = 1$, but spans a range of G_p values depending on the $R_{i,teg}/R_s$ ratio. Increasing the ratio $R_{i,teg}/R_s$ always leads to an increase of G_p at an electrical lossless condition, since a higher $R_{i,teg}$ requires a higher V_{teg} (and consequently P_{teg}) to achieve electrical lossless conditions. Moreover, for both materials the OC case reports higher G_p values at electrical lossless conditions because in this case there is no power loss due to the PV temperature sensitivity.

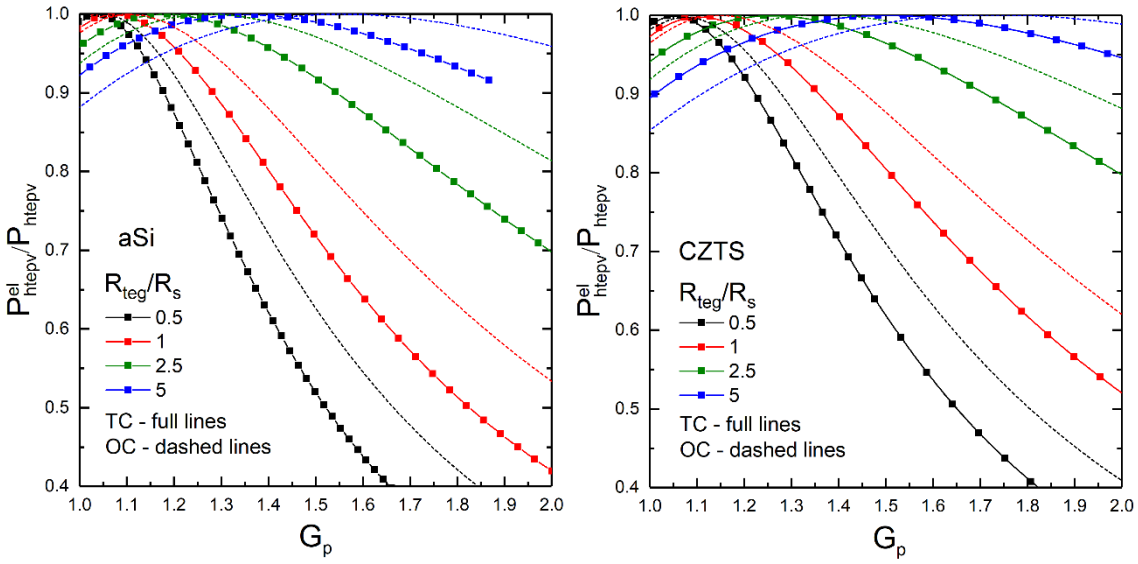

Figure 4. Interplay between electrical losses and G_p for amorphous silicon (a-Si) (**Left**) and copper zinc tin sulfide (CZTS) (**Right**) solar cells. In both plots full and dashed lines refer to thermally coupled (TC) and optically coupled (OC) systems, respectively, while colors refer to different $R_{i,teg}/R_s$ ratios. Simulations were run by sweeping T_{cell} between 300 and 500 K in 5-K steps.

From Figure 4, one may also note that once the electrical lossless condition is reached, any further increase of V_{teg} leads to electrical losses and to a drop of the P^{el}_{htepv}/P_{htepv} ratio. Interestingly enough, such a drop is less pronounced for higher $R_{i,teg}/R_s$ ratios. Specifically, while for $R_{i,teg}/R_s = 0.5$ a change of 15–20 K of the working temperature is sufficient to lead to ≈10% of power losses, for $R_{i,teg}/R_s = 5$, the same change leads to a loss smaller than 2%.

Finally, we remark that G_p only accounts for the ratio between the PV and the TEG power outputs at a given temperature, and should not be confused with the efficiency gain, which is instead the ratio between the PV and TEG efficiencies. Actually, it should be considered that in the calculations T_{cell} was set to range between 300 and 500 K, irrespective of the energy balance between the device temperature and the energy coming from the Sun. Thus, in real situations the incoming solar power could not be large enough to raise the cell temperature to values enabling the gains shown in Figure 4.

4. Discussion

From the results reported in Figures 3 and 4, it is clear that the electrical hybridization of PV and TEG systems is a very delicate matter. The combination of an electrical lossesless condition and a P_{gain} value higher than 1 can only be achieved for a restricted set of working conditions.

In general, it seems that a small PV series resistance along with $R_{i,teg}/R_s$ ratios of around 2.5 leads to the best scenario. In fact, while a small R_s leads to a smaller PV electrical sensitivity, $R_{i,teg}/R_s \approx 2.5$ gives power gains of around 1.2–1.4, representing an achievable aim for this kind of hybrid system [18,19]. It is clear that this combination of parameters is valid for the present case and would generally vary when changing the n_{leg} S_{teg} value of the TEG (namely, changing the thermoelectric material). However, the reported case represents the standard of commercially available TEGs.

Furthermore, the fact that the electrical lossless condition is very sensitive to the device working temperature (namely, the lossless condition occurs only at an optimal V_{teg}) makes electrical hybridization very difficult to implement. In a real-world application, where the solar radiation (and therefore the device temperature) is variable over time, the sensitivity of lossless conditions to V_{teg} (and thus to ΔT) would cause the system to operate in a non-lossless condition most of the time.

A possible solution could be the implementation of an electrical circuit able to monitor electrical losses and to switch between electrical and non-electrical hybridization at convenient times.

5. Conclusions

In this work, an analysis of the influence of various key parameters on the output power of electrically coupled thermoelectric-photovoltaic generators was performed. By means of an apparatus made of a solar cell, a voltage generator, and a variable resistance, the effect of the thermoelectric voltage and its internal resistance were analyzed. Using this apparatus on four silicon solar cells, we showed how a device with a smaller series resistance can better withstand the addition of thermoelectric resistance in the same circuit. We also showed how, consequently, the voltage needed to reach the electrical lossless condition is smaller for solar cells with a smaller series resistance.

Furthermore, using a modified diode equation comprising the effect of the thermoelectric addition and the temperature sensitivity of the solar cell, we studied the relation between the lossless condition and power gain compared to the sole photovoltaic case. Applying the simulations to the case of amorphous silicon and copper zinc thin sulfide, both promising materials for beneficial thermoelectric hybridization, we showed how electrical lossless conditions often do not correspond to significant power gains, in contrast to the sole PV case. We also showed how lossless conditions are strongly temperature-dependent and thus hardly implementable due to their sensitivity to temperature drops in the TEG. This easily drives the system to operate in a non-optimal regime.

Author Contributions: B.L. conceived the work, performed solar cell characterization and wrote the original draft; M.A. performed the simulations, contributed to the data analysis and reviewed the manuscript; D.N. supervised the work, contributed to the data analysis and reviewed the manuscript.

Funding: This project has received funding from the European Union's Horizon 2020 research and innovation program under the Marie Skłodowska-Curie grant agreement No. 745304.

Conflicts of Interest: The authors declare no conflict of interest.

References

1. Chow, T.T. A review on photovoltaic/thermal hybrid solar technology. *Appl. Energy* **2010**, *87*, 365–379. [CrossRef]
2. Yazawa, K.; Shakouri, A. System optimiztion of hot water concentrated solar thermoelectric generation. In Proceedings of the Thermal Issues Emerging Technologies, ThETA 3, Cairo, Egypt, 19–22 December 2010; pp. 283–290.
3. Tyagi, V.V.; Kaushik, S.C.; Tyagi, S.K. Advancement in solar photovoltaic/thermal (PV/T) hybrid collector technology. *Renew. Sustain. Energy Rev.* **2012**, *16*, 1383–1398. [CrossRef]
4. Vorobiev, Y.; González-Hernández, J.; Vorobiev, P.; Bulat, L. Thermal-photovoltaic solar hybrid system for efficient solar energy conversion. *Sol. Energy* **2006**, *80*, 170–176. [CrossRef]
5. Chavez-Urbiola, E.A.; Vorobiev, Y.V.; Bulat, L.P. Solar hybrid systems with thermoelectric generators. *Sol. Energy* **2012**, *86*, 369–378. [CrossRef]
6. Narducci, D.; Lorenzi, B. Challenges and perspectives in tandem thermoelectric-photovoltaic solar energy conversion. *IEEE Trans. Nanotechnol.* **2016**, *15*, 348–355. [CrossRef]
7. Li, Y.; Witharana, S.; Cao, H.; Lasfargues, M.; Huang, Y.; Ding, Y. Wide spectrum solar energy harvesting through an integrated photovoltaic and thermoelectric system. *Particuology* **2014**, *15*, 39–44. [CrossRef]
8. Zhang, J.; Xuan, Y.; Yang, L. Performance estimation of photovoltaic-thermoelectric hybrid systems. *Energy* **2014**, *78*, 895–903. [CrossRef]
9. Liao, T.; Lin, B.; Yang, Z. Performance characteristics of a low concentrated photovoltaic-thermoelectric hybrid power generation device. *Int. J. Therm. Sci.* **2014**, *77*, 158–164. [CrossRef]
10. Bjørk, R.; Nielsen, K.K. The performance of a combined solar photovoltaic (PV) and thermoelectric generator (TEG) system. *Sol. Energy* **2015**, *120*, 187–194. [CrossRef]
11. Cui, T.; Xuan, Y.; Li, Q. Design of a novel concentrating photovoltaic–thermoelectric system incorporated with phase change materials. *Energy Convers. Manag.* **2016**, *112*, 49–60. [CrossRef]
12. Li, D.; Xuan, Y.; Li, Q.; Hong, H. Exergy and energy analysis of photovoltaic-thermoelectric hybrid systems. *Energy* **2017**, *126*, 343–351. [CrossRef]

13. Beeri, O.; Rotem, O.; Hazan, E.; Katz, E.A.; Braun, A.; Gelbstein, Y. Hybrid photovoltaic-thermoelectric system for concentrated solar energy conversion: Experimental realization and modeling. *J. Appl. Phys.* **2015**, *11*. [CrossRef]
14. Luo, B.; Deng, Y.; Wang, Y.; Gao, M.; Zhu, W.; Hashim, H.T. Synergistic photovoltaic–thermoelectric effect in a nanostructured CdTe/Bi_2Te_3 heterojunction for hybrid energy harvesting. *RSC Adv.* **2016**, *6*, 114046–114051. [CrossRef]
15. Yan, X.; Poudel, B.; Ma, Y.; Liu, W.S.; Joshi, G.; Wang, H. Experimental studies on anisotropic thermoelectric properties and structures of n-type $Bi_2Te_{2.7}Se_{0.3}$. *Nano Lett.* **2010**, *10*, 3373–3378. [CrossRef] [PubMed]
16. Xu, L.; Xiong, Y.; Mei, A.; Hu, Y.; Rong, Y.; Zhou, Y. Efficient perovskite photovoltaic-thermoelectric hybrid device. *Adv. Energy Mater.* **2018**, *8*, 1702937. [CrossRef]
17. Narducci, D.; Bermel, P.; Lorenzi, B.; Wang, N.; Yazawa, K. *Hybrid and Fully Thermoelectric Solar Harvesting*, 1st ed.; Springer International Publishing: Cham, Switzerland, 2018.
18. Lorenzi, B.; Contento, G.; Sabatelli, V.; Rizzo, A.; Narducci, D. Theoretical analysis of two novel hybrid thermoelectric–photovoltaic systems based on CZTS solar cells. *J. Nanosci. Nanotechnol.* **2017**, *17*, 1608–1615. [CrossRef] [PubMed]
19. Contento, G.; Lorenzi, B.; Rizzo, A.; Narducci, D. Efficiency enhancement of a-Si and CZTS solar cells using different thermoelectric hybridization strategies. *Energy* **2017**, *131*, 230–238. [CrossRef]
20. Fisac, M.; Villasevil, F.X.; López, A.M. High-efficiency photovoltaic technology including thermoelectric generation. *J. Power Sources* **2014**, *252*, 264–269. [CrossRef]
21. Park, K.T.; Shin, S.M.; Tazebay, A.S.; Um, H.D.; Jung, J.Y.; Jee, S.W. Lossless hybridization between photovoltaic and thermoelectric devices. *Sci. Rep.* **2013**, *3*, 422–427. [CrossRef] [PubMed]
22. Li, G.; Zhou, K.; Song, Z.; Zhao, X.; Ji, J. Inconsistent phenomenon of thermoelectric load resistance for photovoltaic–thermoelectric module. *Energy Convers. Manag.* **2018**, *161*, 155–161. [CrossRef]
23. Verma, V.; Kane, A.; Singh, B. Complementary performance enhancement of PV energy system through thermoelectric generation. *Renew. Sustain. Energy Rev.* **2016**, *58*, 1017–1026. [CrossRef]
24. Cotfas, D.T.; Cotfas, P.A.; Ursutiu, D.; Samoila, C. The methods to determine the series resistance and the ideality factor of diode for solar cells-review. In Proceedings of the 2012 13th International Conference on Optimization of Electrical and Electronic Equipment (OPTIM), Brasov, Romania, 24–26 May 2012; pp. 966–972.
25. Lorenzi, B.; Acciarri, M.; Narducci, D. Conditions for beneficial coupling of thermoelectric and photovoltaic devices. *J. Mater. Res.* **2015**, *30*. [CrossRef]
26. Green, M.A.; Emery, K.; Hishikawa, Y.; Warta, W.; Dunlop, E.D. Solar cell ef fi ciency tables (version 46). *Prog. Photovolt. Res. Appl.* **2015**, *23*, 805–812. [CrossRef]
27. Green, M.A.; Hishikawa, Y.; Warta, W.; Dunlop, E.D.; Levi, D.H.; Hohl-Ebinger, J. Solar cell efficiency tables (version 50). *Prog. Photovolt. Res. Appl.* **2017**, *25*, 668–676. [CrossRef]
28. Kondo, M.; Yoshida, I.; Saito, K.; Matsumoto, M.; Suezaki, T.; Sai, H. Development of highly stable and efficient amorphous silicon based solar cells. In Proceedings of the 28th European Photovoltaic Solar Energy Conference, Villepinte, France, 30 September–4 October 2013; pp. 2213–2217.
29. Sun, K.; Yan, C.; Liu, F.; Huang, J.; Zhou, F.; Stride, J.A. Over 9% efficient kesterite Cu_2ZnSnS_4 solar cell fabricated by using $Zn_{1-x}Cd_xS$ buffer layer. *Adv. Energy Mater.* **2016**, *6*, 1600046. [CrossRef]
30. Sze, S.M. *Physics of Semiconductor Devices*, 2nd ed.; John Wiley & Sons, Ltd.: New York, NY, USA, 1981; pp. 84–89.
31. Friesen, G.; Pavanello, D.; Virtuani, A. Overview of temperature coefficients of different thin film photovoltaic technologies. In Proceedings of the 5th World Conference on Photovoltaic Energy Conversion, Valencia, Spain, 6–10 September 2010; pp. 422–427.
32. Lin, P.; Lin, L.; Yu, J.; Cheng, S.; Lu, P.; Zheng, Q. Numerical simulation of Cu_2ZnSnS_4 based solar cells with In_2S_3 buffer layers by SCAPS-1D. *J. Appl. Sci. Eng.* **2014**, *17*, 383–390.